ASEN 6519: Lidar Remote Sensing - Final Project
Design and Characterization of an Ultraviolet Fluorescence Lidar for the Detection of Biological Aerosols

Name: Loo Ting Tan
Email: lota0178@colorado.edu

Abstract:

In this paper, an UV fluorescence lidar for the detection of biological aerosols is designed and characterized for both day and nighttime operations. The objective is to provide monitoring for biological substances present in the atmosphere that could harm living beings on Earth, to study climate-related impact, or even for national security reasons. Numerical simulation, based on the fluorescence lidar equation, were performed for fluorescence spectra of NADH ranging from 300nm to 800nm, with a frequency-quadrupled Nd:YAG laser exciting the molecules at 266nm. At concentration of 10^6 NADH particles m^{-3} at 20m depth, the lidar system is found to be effective at least up to 2km.

Introduction

The relevance of biological aerosols in atmosphere has been recognized for many years. Biological aerosols in the atmosphere, including bacteria, fungal spores, pollen, viruses, algae etc., can be a concern to human health and can be a significant threat to the environment, and in extreme cases, to human lives when biological warfare is used. There is therefore a need to monitor the aerosols in real-time.

Ultraviolet laser induced fluorescence Lidar has been proposed as a technology for monitoring the presence and concentration of these particles in the atmosphere because many of these bio-aerosols exhibit fluorescence signature in the near-UV spectral range. Therefore, in principle, lasers could be used to induce the fluorescent effects of these biological aerosols. Most of the non-biological aerosols do not exhibit emissions or are weakly fluorescent around these ranges and it therefore allows them to be distinguished. In addition, many biological aerosols have similar excitation wavelength between 260nm to 380nm with typically longer emission wavelengths. This is ideal for classifying different aerosols based on the intensity of the fluorescence spectrum with a single excitation laser.

Fluorescence

Most biological materials contain natural fluorophores, which include aromatic amino acids, nucleic acids, coenzymes such as NADH, flavin etc., vitamin K and congeners (Rao et al., 2017), and they have strong absorption bands in the range between 260 – 380nm while emitting light in the 300 – 800nm range. These natural fluorophores will act as tracers to detect certain biological aerosols.

The occurrence of fluorescence is dependent on the nature of the excited state. In excited singlet states, the electron in the orbital is paired by opposite spin to the second electron in the ground-state orbital. Return to the ground state is therefore spin-allowed and occurs rapidly by emission of a photon. The emission rates of fluorescence are typically 10^8 s^{-1} (lifetime is therefore approximately 10 ns). (Lakowicz, 2010)

Fluorescence generally exhibit a few characteristics. Fluorescence tends to occur at lower energies due to relaxation to lower vibrational states when it is at higher energy levels. Secondly, according to Kasha's rule, fluorescence emission spectrum is generally observed irrespective of the excitation wavelength. The rapid relaxation from higher electronic and vibrational levels to lowest vibrational level typically leads to an

independence of the excitation wavelength. Emission spectrum may vary widely and are dependent upon the chemical structure of the fluorophores and the solvent in which it is dissolved (Lakowicz, 2010).

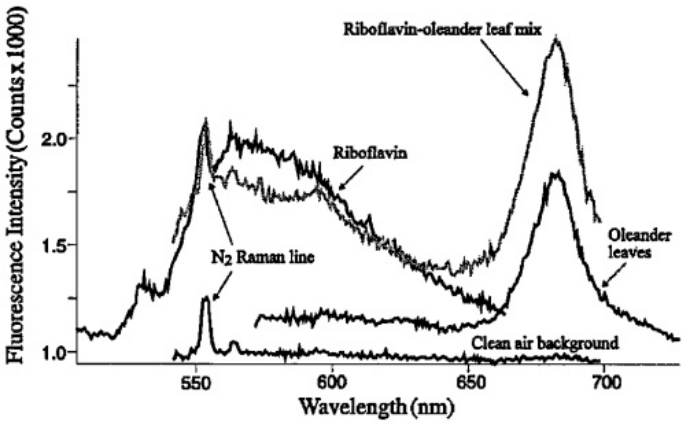

Figure 1: Example of fluorescence spectra of several types of particles made from biological material. (Hill et al., 1995) The N2 Raman line is detectable and serves as a convenient market.

In this project, numerical simulations are performed to evaluate the performance of UV lidar for the detection of Nicotinamide adenine dinucluotide (NADH) with concentration of 10^6 particles spanning a depth of 20m uniformly at different range from 100m to 1900m.

UV-Laser Induced Fluorescence Lidar Architecture

Most atmospheric biological aerosols exhibit strong absorption band at 260 – 380nm and in contrast, non-biological aerosols do not emit fluorescent light in the UV spectral range. A Nd:YAG laser[1] at 1064nm pulse is commonly used for fluorescence lidar and the frequency-quadrupled or -tripled output will allow us to produce a pulse within the desired range at 266nm or 354.7nm. Pulse energies range from few to hundred millijoules in a pulse length of 5-10ns are available commercially. The solid-state lasers are pumped by flash-lamps. Excimer lasers are sometimes used to achieve high repetition rates but, in this application, it will not be required.

The specification is summarized in Table 1:

Table 1: Laser specification

Laser Specification	**Value**
Repetition Rate	10Hz
Energy	60mJ
Pulse width	5-10ns
Divergence	0.5mrads

[1] http://www.dmphotonics.com/NdYAG_FHG/Fourth%20harmonic%20266%20nm%20for%20NdYAG%20laser.htm

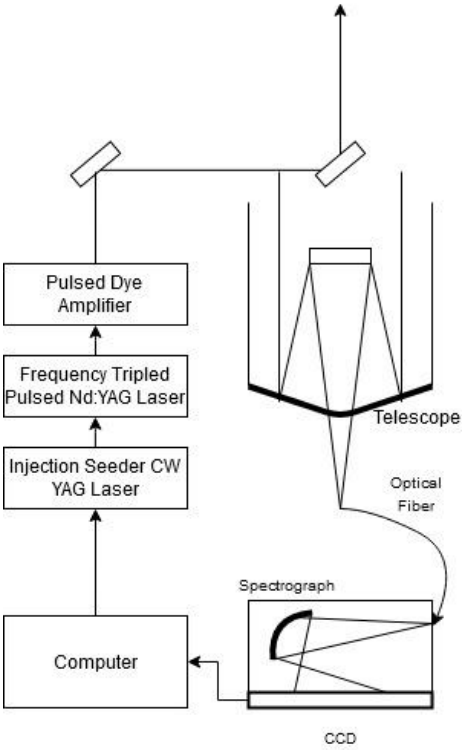

Figure 2: Simplified Schematic of the UV Lidar

In the receiver section, a Cassegrain-type telescope is used where the secondary mirror focuses the fluorescence from the target down into a fiber bundle and be conducted to the entrance slit of a photo-counting multichannel spectrometer and an intensified back-thinned CCD linear sensor. The detector can be time-gated to accept light with the right delay to suppress ambient light, especially solar background which falls in the similar spectral range. The time delay is dependent on the fluorescence lifetime of the target species and a slight delay of 15ns could significantly reduce background solar radiation.

Numerical Simulation

The photon count in the return signal follows the fluorescence resonance lidar equation:

$$N_s(\lambda, z) = \left(\frac{E}{\frac{hc}{\lambda}}\right)\sigma_{abs}(\lambda_L)\Psi(\lambda_L)\int_{\lambda-\frac{\Delta\lambda}{2}}^{\lambda+\frac{\Delta\lambda}{2}} L_F(\lambda')d\lambda' n_c(z)\Delta z \frac{A}{4\pi z^2} T(\lambda_L, z)T(\lambda, z)G(z)\eta(\lambda) + N_B$$

Ozone absorption of 266nm can be significant at higher altitude and therefore should be considered in the attenuation terms if higher altitude is considered. The fluorescence cross-section is typically $10^{-12}m^2$ (Rao et al., 2017). For NADH, the cross section is approximately $5*10^{-12}m^2$.

In comparison to the resonance fluorescence lidar equation below, the key difference lies in the quantum fluorescence yield.

$$N_s(\lambda, z) = \left(\frac{E}{\frac{hc}{\lambda}}\right)\sigma_{sca,eff}(\lambda_L, R)R_B(\lambda)n_c(z)\Delta z \frac{A}{4\pi z^2} T(\lambda_L, z)T(\lambda, z)G(z)\eta(\lambda) + N_B$$

Fluorescence quantum yield $\Psi(\lambda_L)$ is the ratio of the number of photons across the total emission spectra emitted to the number absorbed. It is therefore a function of laser wavelength only. In lower atmosphere, frequent collisional quenching of particles such as oxygen, halogens, or even attenuation by the fluorophore itself could reduce the yield of emitted photons. It is typically 0.1 for bound NADH (Yang et al., 2016).

$L_F(\lambda')$ is the normalized fluorescence spectra and is integrated across the normalized fluorescence spectra around the mean based on the filter bandwidth $\Delta\lambda$. It is similar to the branching ratio term in the resonance fluorescence lidar equation. Typically, log-normal description of fluorescence spectra of organic fluorophores (e.g. tryptophan, quinine etc.) is a good analytical description of these simpler molecules (Burstein & Emelyanenko, 1996). Molecules with more complex vibrational structures would exhibit a non-log-normal shapes as shown in Fig. 3 (Top). The equations and parameters used to model NADH's emission are as follow (Table 2).

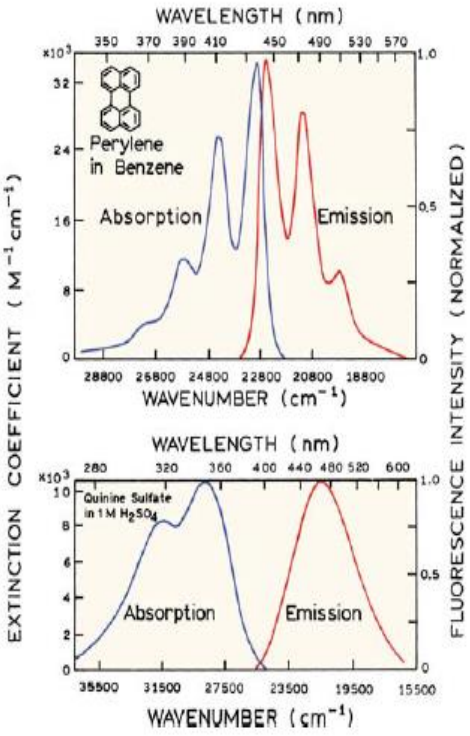

Figure 3: Molecules with more vibrational structure (Top) does not exhibit a log-normal emission spectra (Lakowicz, 2006)

$$I(\upsilon) = I_m \exp\left\{-\frac{\ln 2}{ln^2\rho} ln^2\left(\frac{a-\nu}{a-\nu_m}\right)\right\}$$

$$\rho = \frac{\nu_m - \nu_-}{\nu_+ - \nu_m}$$

$$a = \frac{\nu_m + H\rho}{\rho^2 - 1}$$

$$H = \nu_+ - \nu_-$$

Table 2: NADH Log-normal Equation Parameters

	ν_m (10^3 cm^{-1})	ν_+ (10^3 cm^{-1})	ν_- (10^3 cm^{-1})
NADH	21.80	23.86	19.29

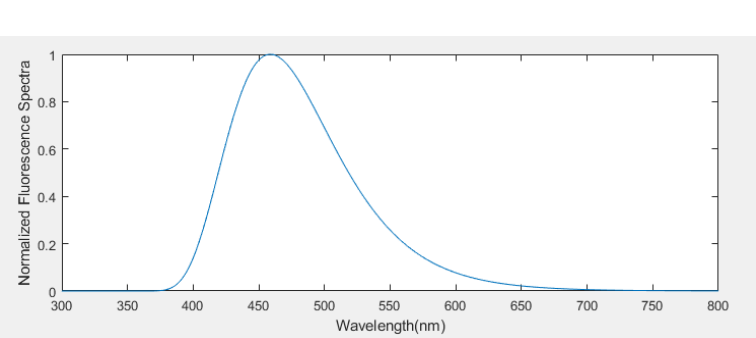

Figure 4: Comparison of the NADH log-normal equation vs experimental data. NADH has a peak emission at 450.

$$T(\lambda, z) = exp\left(-\int_0^Z \alpha(\lambda, r)dr + \int_{Z_{layer\ start}}^{Z_{layer\ ends}} \alpha_c(\lambda, r)dr\right)$$

$$\alpha = \alpha_{mol.scattering} + \alpha_{mol,abs} + \alpha_{aer,scattering} + \alpha_{aer,abs}$$

Rayleigh and Mie scattering are considered in the following empirical equations (Hong et al. 2005) to account for atmospheric attenuation:

$$\alpha_{mol}(\lambda, z) = \frac{8\pi}{3} \times 1.54 \times 10^{-3} \exp\left(-\frac{z}{7}\right) \left(\frac{532}{\lambda(nm)}\right)^4$$

$$\alpha_{aer}(\lambda, z) = 50\left(2.47 \times 10^{-3} \exp\left(-\frac{z}{2}\right) + 5.13 \times 10^{-3} \exp\left(-\frac{(z-20)^2}{36}\right)\right)\left(\frac{532}{\lambda(nm)}\right)$$

Extinction due to the constituents NADH can similarly be separated into excitation and emission components. For excitation at 266nm, Beers-Lambert's law is used to approximate the transmission losses in the constituent layer L. Given the molar attenuation coefficient at 16,900 M^{-1} cm^{-1}, the following equation could be used to obtain the excitation transmission. The transmission losses are found to be near 0 due to the thin layer of the NADH samples assumed. If large depth and concentration of the samples are present in the atmosphere, the extinction due to the constituents would become significant.

$$T_{exc,\ 266nm} = \exp\left(-16{,}900 * M * \frac{n_c}{N_A} L\right)$$

$$M_{NADH} = 663.43 g/mol$$

For the attenuation for emission, experimental data of the NADH extinction as a function of wavelength from literature has been unavailable. However, from the Figure 5 below, it is observed that the absorbance of NADH is approximately 0 above 400nm, and the spectral range of interest in NADH emission lies above 400nm. Therefore, it assumed that there is no extinction on the emission wavelengths (T=1).

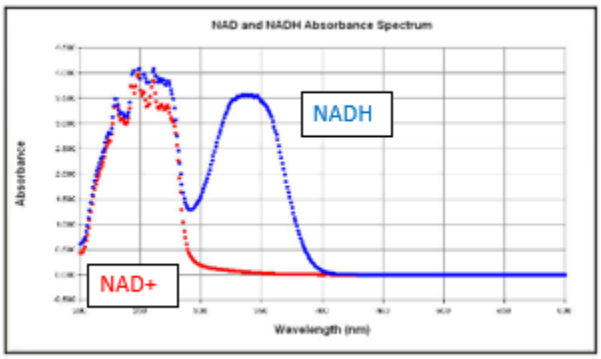

Figure 5: Experimental absorbance data of NADH and NAD+. The absorbance above 400 is 0 for the frequencies of interests.

In general, lidar performance in terms of signal to noise ratio would be adversely affected due to the intense background noise in the range of 300-800nm. It is however necessary to develop a system suitable for real-time monitoring of aerosols during daytime as well. A synchronous-delay detection technique will be necessary to operate the UV lidar during daytime. We approximate nighttime background count to be approximately 0.

The background noise count is obtained using the following equations (Nakajima et al., 1999

$$N_B = \frac{S(\lambda)}{4\pi} \frac{\lambda}{hc} A_{rec} \eta_{qde}(\lambda) \eta_{opt}(\lambda) \Delta t \Delta\lambda \frac{FOV^2}{2} \pi$$

Spectral irradiance $S(\lambda)$ is plotted with the corresponding background photon count for comparison in Figure 6. The higher wavelength photon count is approximately constant despite the slower decrement in spectral irradiance with respect to the wavelength.

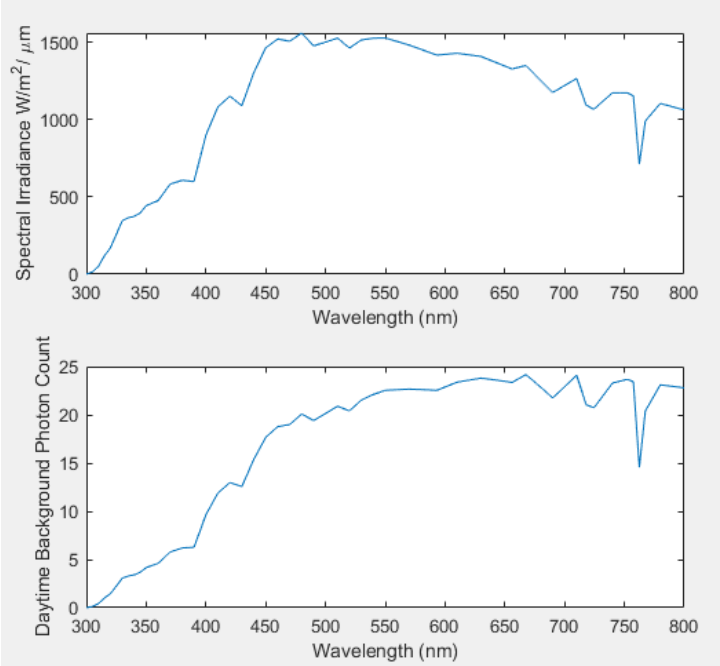

Figure 6: Solar spectral Irradiance (Top) is used to compute the daytime background photon count (Bottom).

Dark current noise N_D from photo-counting spectrometers are not insignificant and has to be considered. The integration time for both background count is based on the depth of the sample in the atmosphere or region of interest.

$$N_D = CSP \cdot \Delta t$$

$$\Delta t = 2 \cdot depth/c$$

The parameters used for the simulation are summarized in the Table 3 below.

Table 3: Simulation Parameters

Simulation Parameters	**Value**
Pulse energy	60mJ
Excitation Wavelength	266nm
Receiver spectral bandwidth	300 to 800nm
Transmitter Optics efficiency	0.98^3
Quantum efficiency	0.4
CCD Efficiency (300 - 800nm)	1
Field of View	0.5 mrad
Receiver diameter	81cm
Receiver Optics and Fiber efficiency	0.9^3
Spectrometer bandwidth	5nm
Dark Current	$500s^{-1}$
Quantum Yield (NADH)	0.1
Absorption Cross section (NADH)	$5 * 10^{-12}$ m^2

Discussion

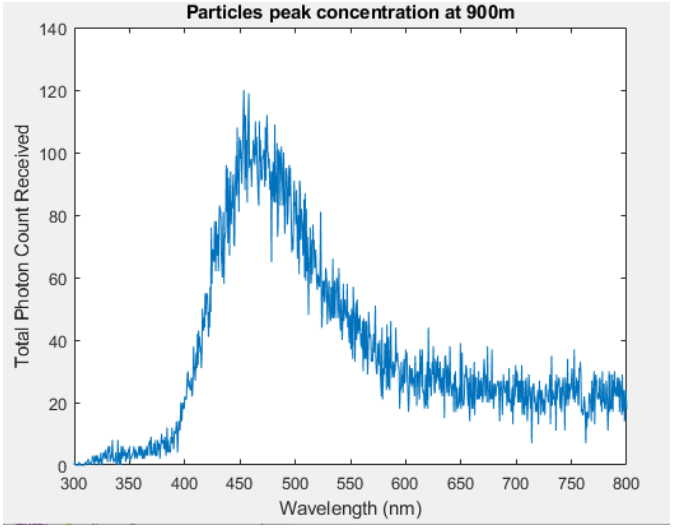

Figure 7: Single shot photon count with particles cloud at 900m with respect to wavelength

Signal-to-noise ratio can be computed with the equation as follows:

$$SNR(z) = \frac{N_s(z)}{\sqrt{N_s(z) + 2(N_b + N_d)}}\sqrt{n}$$

In Figure 8, the SNR is plotted as a function of wavelength for various peak locations of NADH samples in the atmosphere ranging from 100m to 1900m. From 100m to 1900 m, it is observed that the NADH signals at 10^6 particles m^{-3} are still detectable. At ranges further than 1900m with signals marginally higher than background noise, time integration of signals may be used to improve SNR.

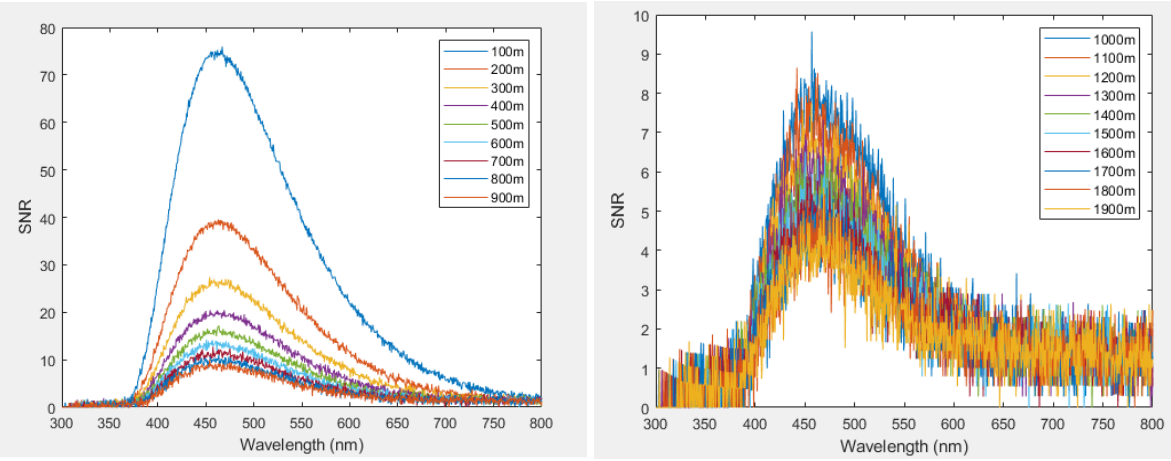

Figure 8: Signal to Noise Ratio Plot at different ranges.

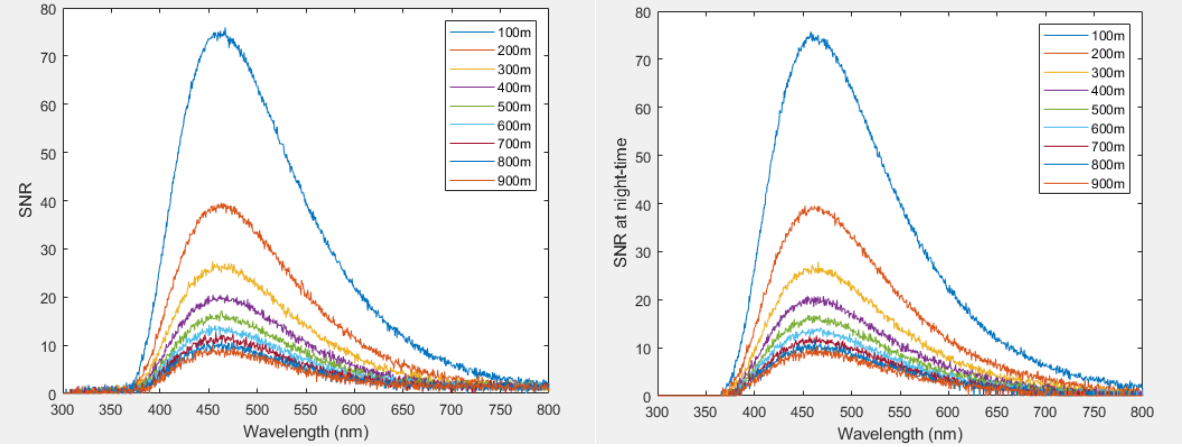

Figure 9: SNR comparison between daytime and nighttime. Nighttime SNR is slightly improved in SNR.

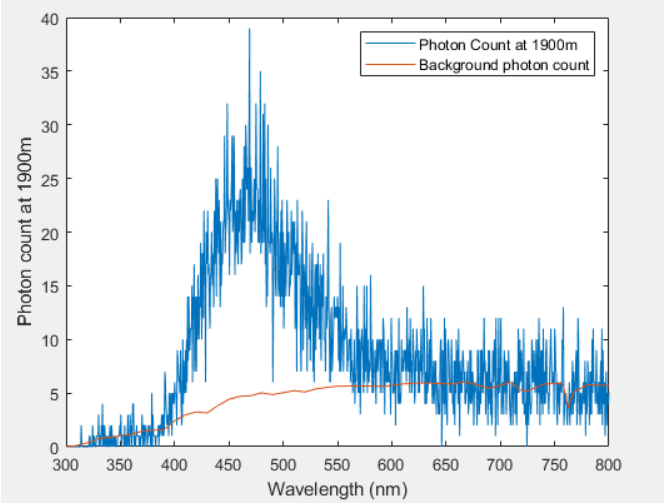

Figure 10: Single-Shot photon count at 1900m and daytime background noise.

Summary

In this paper, a UV fluorescence lidar to detect biological aerosols is designed and characterized using simulation. The SNR of NADH emission between 0km to 2km is investigated. Preliminary numerical results suggest that with 60mJ of laser, the NADH at 10^6 m^{-3} at a depth of 20m is still detectable even in daytime. It is also essential to understand the effect of higher laser power on changing the chemical structure of the molecules of interest.

For future work, an investigation of the minimal detectable concentrations should be conducted to provide a better understanding of the effectiveness of the instrument. Various biological aerosols should also be considered in order to establish a database for future lidar development and applications.

Reference

Burstein, E. A., Emelyanenko, V. I. (1996) Log-Normal Description of Fluorescence Spectra of Organic Fluorophores. *Photochemistry and Photobiology*, 1996, 64 (2): 316-320

Lakowicz, J. R. (2010). *Principles of fluorescence spectroscopy*. New York: Springer Science+Business Media.

Nakajima, T.Y., Imai, T., Uchino, O., Nagai, T. (1999) Influence of daylight and noise current on cloud and aerosol observations by spaceborne elastic scattering lidar. *Applied optics* (1999) Vol. 38 No. 24

Pan, Y.L. (2015) Detection and Characterization of biological and other organic-carbon aerosol particles in atmosphere using fluorescence. *Journal of Quantitative Spectroscopy and Radiative Transfer* (2015) Vol. 150, pp. 12- 35

Rao, Z., Hua, D., He, T., Wang, Q., Le, J. (2017) Effects of intrinsic fluorescence on biological aerosols detection accuracy of lidar. *Measurement* 106 (2017) pp. 12-17.

Hong, G., Zhang, Y., Zhao, Y., Shao, S., Tan, K., Hu, H. (2006) Raman lidar for profiling atmospheric CO2. *Acta Physica Sinica* (2006). Vol 55, No.2

Passarella, S., Dechecchi, M.C., Quagliariello, E. (1981) Optical and Biochemical Properties of NADH Irradiated by High Peak Power Q-Switched Ruby Laser or Low Power C.W. HeNe Laser. *Bioelectrochemistry and Bioenergetics* (1981) Vol 128, pp. 315-326.

Appendix: Simulation Matlab Code

```
clear; clc; close all;
% Lidar Final Project 2020 - UV fluorescence lidar for the detection of
% Biological aerosols
% Loo Ting Tan
% lota0178@colorado.edu/ tanlooting@hotmail.com

pi=3.14159265;
h=6.626070040E-34;
c=2.99792458e8;                 % light speed (m/s)
Oss=0.641;                      % Oscillator strength for Na D2 line
kB=1.3806508e-23;               % Boltzmann constant (Unit:  J/K)
Qe=1.60217733e-19 ;

%laser constants
l_e = 60E-6; %mJ
laser_wl = 355E-9; %nm
d_wl = 5; %filter bandwidth [nm]
r_A= pi()*(0.81/2)^2; %telescope area [m]
fov = 0.5; %mrad
sigma =1E-12; % average fluorescence cross section
T_trans=0.8;
R_trans =0.9*0.85*0.9*0.9;
phi = 0.1; %quantum fluorescence yield
csp = 500; % [s-1] dark noise current
qde= 0.4; % from HW should be one?

r_step=0.5;
range = 1:r_step:1000; %2km
peak_loc= 100:100:900;
for po = 1:length(peak_loc)
    % number density
    dep= 20; %20m

    rho= 10E6; % cloud density
    start_i=find(range==peak_loc(po));
    n_d= zeros(size(range));
    n_d(start_i:start_i+dep/r_step -1)= rho/(dep/r_step); % assume gaussian

    step = 0.5;
    wl = 100:step:1000;
    wl2= 300:step:800;
    % linear function of UV fingerprint

    d_w=10;
    %wle=450;
    %l_wl= 2/(d_w)*sqrt(log(2)/pi())*exp(-4*log(2)*((wl - wle)/d_w).^2);

    %% normalized fluorescence spectra - trytophan
    vplus = 1e7/23.86e3;
    vminus = 1e7/19.29e3;
    vmax = 1e7/21.80e3;
    p=(vmax-vminus)/(vplus-vmax);
    hf = vplus-vminus;
    a= vmax+hf*p/(p^2-1);
    l_wl = exp(-(log(2)/(log(p)^2))*abs(log((a-wl)/(a-vmax))).^2);

    %%
    for j=1:length(wl2) %emission wavelength

        cum_i=find(wl==wl2(j));
        cum_l_wl(:,j)=sum(l_wl(cum_i-d_w/2/step:cum_i+d_w/2/step))*d_w;
        %plot(wl, l_wl);

        a_m_l = 8*pi()/3*1.54e-3*exp(-range/7)*((532/(laser_wl*1E9))^4);
        a_am_l = 50*((2.47*1E-3*exp(-range/2)+5.13E-6*exp(-(range-
20).^2/36)))*532/(laser_wl*1E9);
        a_m_e = 8*pi()/3*1.54e-3*exp(-range/7)*((532/(wl2(j)))^4);
        a_am_e = 50*((2.47*1E-3*exp(-range/2)+5.13E-6*exp(-(range-20).^2/36)))*532/(wl2(j));
        total_u = a_m_l+a_am_l;
```

```
        total_d=a_m_e + a_am_e;
        for k = 1: length(range)
                trans_t_u(k)= exp(-sum(total_u(1:k))*r_step);
                trans_t_d(k,j)= exp(-sum(total_d(1:k))*r_step);
        end
        %extinction spectra for NADH
    end

    a_c_l= exp(-16900*1E2*rho*dep/(6.022E23));

    %% Total Photon Count for each wavelength
    dcs = (phi*sigma*cum_l_wl).*(n_d)';
    ph_c=
((l_e*laser_wl/h/c)*(r_A./(4*pi()*range.^2))'*(T_trans*R_trans*qde).*(dcs).*trans_t_u').*(trans
_t_d)*a_c_l;

    for i = 1:length(wl2)
        tot_ph_c(po,i)= nansum(ph_c(:,i));
    end
end
%figure(2);
%plot(wl2,tot_ph_c);xlabel("Wavelength(nm)"); ylabel("Total Photon Count (excl. bg and dark
current noise");
%% Daytime background
d_T = 2*dep/c;

spec=xlsread("C:\Users\tanlo\Documents\ASEN\Sem3 - Lidar Remote
Sensing\HW\project\spectral_irrad.xlsx");
wl_s=spec(:,1)*1000;
s_irrad = spec(:,2);
s_irrad_interp= interp1(wl_s,s_irrad,wl2);
figure(3);
subplot(2,1,1);
plot(wl2,s_irrad_interp);xlabel("Wavelength (nm)"); ylabel("Spectral Irradiance W/m^2/ \mum")
nb = s_irrad_interp.*wl2*1E-6*(fov*0.001/2)^2*pi()*qde*r_A*d_T*(d_wl*1E-9)*R_trans/h/c/4/pi();
subplot(2,1,2);
plot(wl2,nb); xlabel("Wavelength (nm)"); ylabel("Daytime Background Photon Count");

% dark current noise
nd = csp*d_T;
%% Total Signal
[row, col] = size(tot_ph_c);
for m = 1:row
    Nt(m,:)=poissrnd(tot_ph_c(m,:))+poissrnd(nb)+nd;
end
figure(4);
plot(wl2,Nt(10,:)); hold on; plot(wl2,nb);  xlabel("Wavelength (nm)"); ylabel("Photon count at
1900m"); legend("Photon Count at 1900m", "Background photon count");
%% Sensitivity analysis
shotsnum=1;
figure(5);
for b= 1:length(peak_loc)
    snr(b,:)= sqrt(shotsnum)*Nt(b,:)./sqrt(Nt(b,:)+2*(nb+nd));

end
plot(wl2,snr); xlabel("Wavelength (nm)"); ylabel("SNR at night-time");
```